Angiogenesis precedes myogenesis during regeneration following biopsy injury in skeletal muscle

Nicole L. Jacobsen[1]†, Aaron B. Morton[1]†, Steven S. Segal[1-4]*

[1]Department of Medical Pharmacology and Physiology, University of Missouri; Columbia, MO

[2]Dalton Cardiovascular Research Center; Columbia, MO

[3]Department of Biomedical Sciences, University of Missouri; Columbia, MO

[4]Department of Biomedical, Biological, and Chemical Engineering, University of Missouri; Columbia, MO

*Corresponding author. Email: segalss@health.missouri.edu

†These authors contributed equally to this work.

Abstract

Acute injury to skeletal muscle damages myofibers and fragments capillaries which then regenerate to restore intact muscle. However, it is unknown whether these processes are concomitant or proceed sequentially. We find that following punch biopsy of skeletal muscle in adult mice, which removes all tissue components, a provisional matrix fills the wound within 1 day post injury (dpi). Microvessels infiltrate the matrix by 7 dpi, with perfused networks traversing the wound by 14 dpi. In contrast, the wound is devoid of myofibers at 7 dpi. Myofibers begin regenerating into the wound at 14 dpi and span the wound by 21 dpi. We conclude that angiogenesis precedes myogenesis following skeletal muscle biopsy injury and suggest that a vascular supply supports myofiber regeneration.

One-Sentence Summary

The microcirculation is restored prior to the regeneration of myofibers following biopsy injury of skeletal muscle.

Main Text

Acute injury to skeletal muscle damages myofibers, triggers an inflammatory response, and fragments capillary networks. Although the events and time course of inflammation (*1*) and the regeneration of myofibers from resident muscle stem cells (*2*) are well defined, data regarding the recovery of the microcirculation following injury are limited. Capillaries can regenerate from surviving endothelial cells into disordered networks which reorganize as the regenerated myofibers mature (*3-5*). However, it is unknown whether microvascular regeneration and myofiber regeneration are concomitant processes or proceed sequentially following injury to adult skeletal muscle.

To investigate this relationship, we developed a model of complete tissue removal from the gluteus maximus (GM) muscle of male and female adult mice. The GM is a thin muscle (thickness, ~200 μm) of mixed fiber type (*6*) that is amenable to high resolution imaging of the microcirculation at defined stages of myofiber regeneration following local exposure to the myotoxin $BaCl_2$ (*3-5*). In contrast to traumatic injury induced by myotoxins, crushing, or extreme cold (*7*) where cellular debris are removed by efferocytosis and basal laminae persist (*8*) punch biopsy completely removes a designated volume of all tissue components, creating an empty gap into which regeneration proceeds (*9*). As reported here, this experimental approach resolves angiogenesis from myogenesis in adult skeletal muscle, thereby permitting detailed study of the temporal relationship between regeneration of myofibers and their vascular supply for the first time. We hypothesized that following removal of all tissue components, angiogenesis precedes the formation of new myofibers to support the metabolic demands of regenerating skeletal muscle.

Local injury was created using a biopsy punch (diameter, 2 mm) to remove a volume of the GM that is below the critical threshold for regeneration following volumetric muscle loss [Fig.

1A; (*10*)]. Punch biopsy produces a circular hole through the center of the GM with minimal damage to the surrounding tissue; nominal uptake of Evans Blue dye into the ends of myofibers bordering the wound was apparent at 1 day post injury (dpi; Supp. Fig. 1). Intravascular injection of fluorescent dextran (mass, 70 kDa) confirmed a void within the wound while preserving microvascular perfusion surrounding the injury (Fig. 1B).

Sirius red staining revealed the deposition of collagen to create a provisional matrix that spanned the wound at 1 dpi (Fig. 1C). The provisional matrix was invaded by PDGFRα^{+} cells accompanied by CD45^{+} inflammatory cells (Fig. 1D). Fibroadipogenic precursor cells (FAPs) express PDGFRα and have the ability to differentiate into fibroblasts and adipocytes but not into muscle stem cells (satellite cells) or myofibers (*11*). Identified by the expression of mesenchymal stem cell surface proteins (e.g., PDGFRα, CD34, and Sca-1), FAPs reside in the interstitial space of healthy skeletal muscle (*12*). Upon injury, FAPs enter the cell cycle to proliferate, localize to the site of tissue damage, differentiate, and promote myogenesis. Activated FAPs deposit ECM proteins, secrete myogenic differentiation factors, and recruit CD45^{+} immune cells via paracrine signaling (*11*). The ensuing cascade of granulocytes, monocytes, and macrophages produce cytokines and chemokines aimed at clearing cellular debris, promoting self-renewal of satellite cells, and preventing premature myogenic cell differentiation (*1*). Thus, the microenvironment of the provisional ECM established by FAPs and immune cells serves as the foundation for the regeneration of intact skeletal muscle.

Using an endothelial cell (EC)-specific Cre driver [Cdh5-Cre^{ERT2}; (*13*)] and tamoxifen-induced recombination of the Rosa26^{mTmG} locus to genetically label the endothelium with membrane-bound eGFP (Cdh5-mTmG mice), we evaluated microvascular regeneration following punch biopsy. Angiogenic sprouting was apparent as early as 5 dpi (not shown) and began extending into the wound at 7 dpi (Fig. 2A&B). Specialized endothelial tip cells guide capillary

sprouts as they sense attractive and repulsive signals in their surroundings while stalk cells proliferate behind tip cells to elongate newly forming capillaries (*14*). Nascent vessels also underwent internal division (i.e., intussusceptive angiogenesis) as microvascular networks divided and extended across the wound at 10 dpi (Fig. 2C&D). This mechanism of revascularization was recently reported to be the dominant mechanism of regenerative angiogenesis following hindlimb ischemia (*15*). Through 14 dpi, microvessels would split into two daughter vessels and thereby generate numerous branches with short interconnections and without associated sprouting points (Fig. 2E). Vasculogenesis may also contribute to revascularization after biopsy injury but was not resolved in these experiments. Nevertheless, a centripetal gradient of microvessel growth, from the edges towards the center of the wound, was manifest from 7-14 dpi.

Perfused microvascular networks spanned the wound by 14 dpi but lacked hierarchical structure or definitive patterns of blood flow (Fig. 3, Supp. Fig. 2). Instead, nascent microvessel diameters were enlarged and clustered into zones of angiogenic activity. The diameter of microvessels significantly increased from 4.1 ± 0.3 μm in uninjured muscle to 7.4 ± 0.4 μm and 9.0 ± 0.6 μm at 7 dpi and 14 dpi, respectively (Fig. 3D). Intravital microscopy revealed that only the microvessels having the largest diameter were continuously perfused; most segments contained stationary red blood cells (RBCs) or plasma alone at 14 dpi (Supp. Fig. 2). In perfused microvessels, the direction of blood flow oscillated and was interspersed with periods of flow cessation. These aberrant patterns of perfusion can be attributed to the lack of hierarchical organization in newly forming networks or established arterio-venous pressure gradients (*16*).

By 21 dpi, extensive microvascular networks encompassed the site of injury (Fig. 3E) and microvessel diameter nearly recovered to control values (6.6 ± 0.8 μm). Nevertheless, the parallel arrangement of microvessels observed in uninjured skeletal muscle was not restored. Instead, numerous anastomoses created circuitous pathways for local blood flow. The absence of

microvascular reorganization otherwise seen during regeneration following myotoxin injury (*4*) may be attributable to the loss of spatial cues otherwise provided by residual basal lamina (*8*).

In striking contrast to the time course of revascularization, the wound remained devoid of myofibers at 7 dpi, a time at which myofiber regeneration would be well advanced after other skeletal muscle injury models (*5, 7*). As they began to penetrate the provisional matrix and regenerate into the wound at 10-14 dpi (Fig. 3), myofibers were densely packed, interwoven, smaller in diameter, and coursed alongside the wound edge before integrating with undamaged myofibers. That regenerating myofibers intertwine instead of exhibiting their characteristic parallel alignment further suggests that the provisional matrix lacks the structural basis otherwise provided by the residual basal laminae, which was removed by the punch biopsy (*8, 17*).

Newly formed myofibers spanned the wound at 21 dpi, but clusters of adipocytes displaced muscle tissue where myofibers had not yet completely regrown (Fig. 3C, Supp. Fig. 3). If myoblast migration and fusion are delayed, multipotent FAPs may contribute to fibrosis and fat infiltration (*18*). In turn, regenerating capillary networks remodeled in accord with adipocyte morphology (Fig. 3C). Taken together, the present data indicate that revascularization precedes the replacement of myofibers following punch biopsy and that loss of skeletal muscle ultrastructure disrupts the morphology of regenerating tissue components.

To confirm that revascularization occurred prior to myofiber regeneration, GM cross sections (thickness, 10 μm) were immunolabeled for CD31 to identify ECs, myosin heavy chain (MyHC) for contractile myofibers, laminin to detect basal laminae, and DAPI for nuclei. Congruent with data from intravital and confocal imaging, healing progressed into the wound from 7 dpi through 21 dpi (Fig. 4). Newly forming myofibers within the wound were smaller than uninjured myofibers. Remarkably, not all regenerating myofibers contained central nuclei, a

hallmark of muscle regeneration (*2*). Instead, the nuclei of many regenerated fibers were located at the periphery, which is typical of uninjured myofibers (Fig. 4F). This difference in nuclear localization following punch biopsy implicates a modified mechanism of myogenesis when compared to other models of skeletal muscle injury and myofiber regeneration (*19*), and instead resembles *de novo* myogenesis in the embryo. The size of the injured region devoid of myofibers (i.e., diameter of remaining visible wound) was used as an index of healing over time. This distance was 1512 ± 153 μm at 7 dpi which progressively decreased to 475 ± 134 μm and 71 ± 71 μm at 14 and 21 dpi, respectively. We quantified the area occupied by ECs within the region lacking myofibers as an indicator of microvascular density that preceded myogenesis into the wound. The EC area was 2794 ± 1126 μm^2 at 7 dpi and 3366 ± 930 μm^2 at 14 dpi but decreased to 700 ± 700 μm^2 at 21 dpi, reflecting the growth of myofibers into the wound as regeneration advanced.

Skeletal muscle has a remarkable capacity to regenerate following injury. Our goal was to determine whether the regeneration of myofibers and microvessels proceeded sequentially or simultaneously. Creating a hole through the entire muscle enabled definitive temporal resolution of angiogenesis versus myogenesis for the first time. Following punch biopsy injury, a provisional matrix invested with inflammatory cells and fibroblasts is deposited within 1 dpi. Sprouting and intussusceptive angiogenesis revascularize the wound and begin prior to the emergence of regenerating myofibers. Consistent with other models of injury, intact muscle invested with a microvascular supply is restored by 21 dpi. With numerous pathological conditions involving aberrant regulation of myogenesis and/or angiogenesis, the present data support the hypothesis that re-establishing a microvascular network is integral to effective regeneration of intact, functional skeletal muscle.

References and Notes

Materials and methods are available as supplementary materials at the Science website.

1. J. G. Tidball, Regulation of muscle growth and regeneration by the immune system. *Nat Rev Immunol* **17**, 165-178 (2017).
2. H. Yin, F. Price, M. A. Rudnicki, Satellite cells and the muscle stem cell niche. *Physiol Rev* **93**, 23-67 (2013).
3. A. B. Morton *et al.*, Barium chloride injures myofibers through calcium-induced proteolysis with fragmentation of motor nerves and microvessels. *Skelet Muscle* **9**, 27 (2019).
4. N. L. Jacobsen, C. E. Norton, R. L. Shaw, D. D. W. Cornelison, S. S. Segal, Myofibre injury induces capillary disruption and regeneration of disorganized microvascular networks. *J Physiol* **600**, 41-60 (2022).
5. C. A. Fernando, A. M. Pangan, D. Cornelison, S. S. Segal, Recovery of blood flow regulation in microvascular resistance networks during regeneration of mouse gluteus maximus muscle. *J Physiol* **597**, 1401-1417 (2019).
6. S. J. Lampa, S. Potluri, A. S. Norton, M. B. Laskowski, A morphological technique for exploring neuromuscular topography expressed in the mouse gluteus maximus muscle. *Journal of Neurosci Methods* **138**, 51-56 (2004).
7. D. Hardy *et al.*, Comparative Study of Injury Models for Studying Muscle Regeneration in Mice. *PLoS One* **11**, e0147198 (2016).

10. S. E. Anderson *et al.*, Determination of a Critical Size Threshold for Volumetric Muscle Loss in the Mouse Quadriceps. *Tissue Eng Part C Methods* **25**, 59-70 (2019).

11. B. Biferali, D. Proietti, C. Mozzetta, L. Madaro, Fibro-Adipogenic Progenitors Cross-Talk in Skeletal Muscle: The Social Network. *Front Physiol* **10**, 1074 (2019).

12. A. W. Joe *et al.*, Muscle injury activates resident fibro/adipogenic progenitors that facilitate myogenesis. *Nat Cell Biol* **12**, 153-163 (2010).

13. Y. Wang *et al.*, Ephrin-B2 controls VEGF-induced angiogenesis and lymphangiogenesis. *Nature* **465**, 483-486 (2010).

14. R. Blanco, H. Gerhardt, VEGF and Notch in tip and stalk cell selection. *Cold Spring Harb Perspect Med* **3**, a006569 (2013).

15. J.-M. Arpino *et al.*, Low-flow intussusception and metastable VEGFR2 signaling launch angiogenesis in ischemic muscle. *Sci Adv* **7**, eabg9509 (2021).

16. A. R. Pries, T. W. Secomb, Making microvascular networks work: angiogenesis, remodeling, and pruning. *Physiology (Bethesda)* **29**, 446-455 (2014).

17. J. R. Sanes, The Basement Membrane/Basal Lamina of Skeletal Muscle. *J Biol Chem* **278**, 12601-12604 (2003).

18. M. W. Hamrick, M. E. McGee-Lawrence, D. M. Frechette, Fatty Infiltration of Skeletal Muscle: Mechanisms and Comparisons with Bone Marrow Adiposity. *Front Endocrinol (Lausanne)* **7**, 69 (2016).

19. E. S. Folker, M. K. Baylies, Nuclear positioning in muscle development and disease. *Front Physiol* **4**, 363 (2013).

20. H. S. Baldwin *et al.*, Platelet endothelial cell adhesion molecule-1 (PECAM-1/CD31): alternatively spliced, functionally distinct isoforms expressed during mammalian cardiovascular development. *Development* **120**, 2539-2553 (1994).

21. F. Biscetti *et al.*, High-mobility group box-1 protein promotes angiogenesis after peripheral ischemia in diabetic mice through a VEGF-dependent mechanism. *Diabetes* **59**, 1496-1505 (2010).

22. D. G. Gilbertson *et al.*, Platelet-derived growth factor C (PDGF-C), a novel growth factor that binds to PDGF alpha and beta receptor. *J Biol Chem* **276**, 27406-27414 (2001).

23. D. Bader, T. Masaki, D. A. Fischman, Immunochemical analysis of myosin heavy chain during avian myogenesis in vivo and in vitro. *J Cell Biol* **95**, 763-770 (1982).

24. N. C. Bal *et al.*, Both brown adipose tissue and skeletal muscle thermogenesis processes are activated during mild to severe cold adaptation in mice. *J Biol Chem* **292**, 16616-16625 (2017).

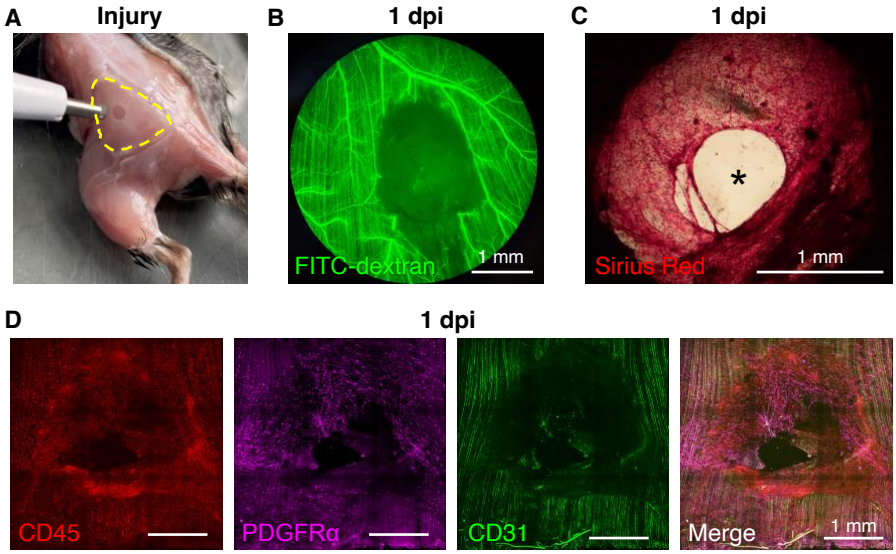

Figure 1. Punch biopsy removes all skeletal muscle tissue components. **A.** A biopsy punch was used to create a local injury (diameter, 2 mm) through the GM of male and female mice. **B.** Microvascular perfusion was disrupted at the site of the injury at 1 dpi. Intravascular injection of FITC-conjugated dextran (mass, 70 kDa) showed the empty biopsy site with a small unperfused region downstream of the injury. **C.** Representative Sirius red staining of collagen at 1 dpi highlighting deposition of a provisional matrix in the wound; * indicates residual gap. **D.** Stitched tile scan of immunostained whole mount GM at 1 dpi showing masses of inflammatory cells ($CD45^+$, red) and fibroblasts ($PDGFR\alpha^+$, magenta) invading the provisional matrix; capillaries ($CD31^+$, green) retain parallel orientation along surrounding uninjured myofibers.

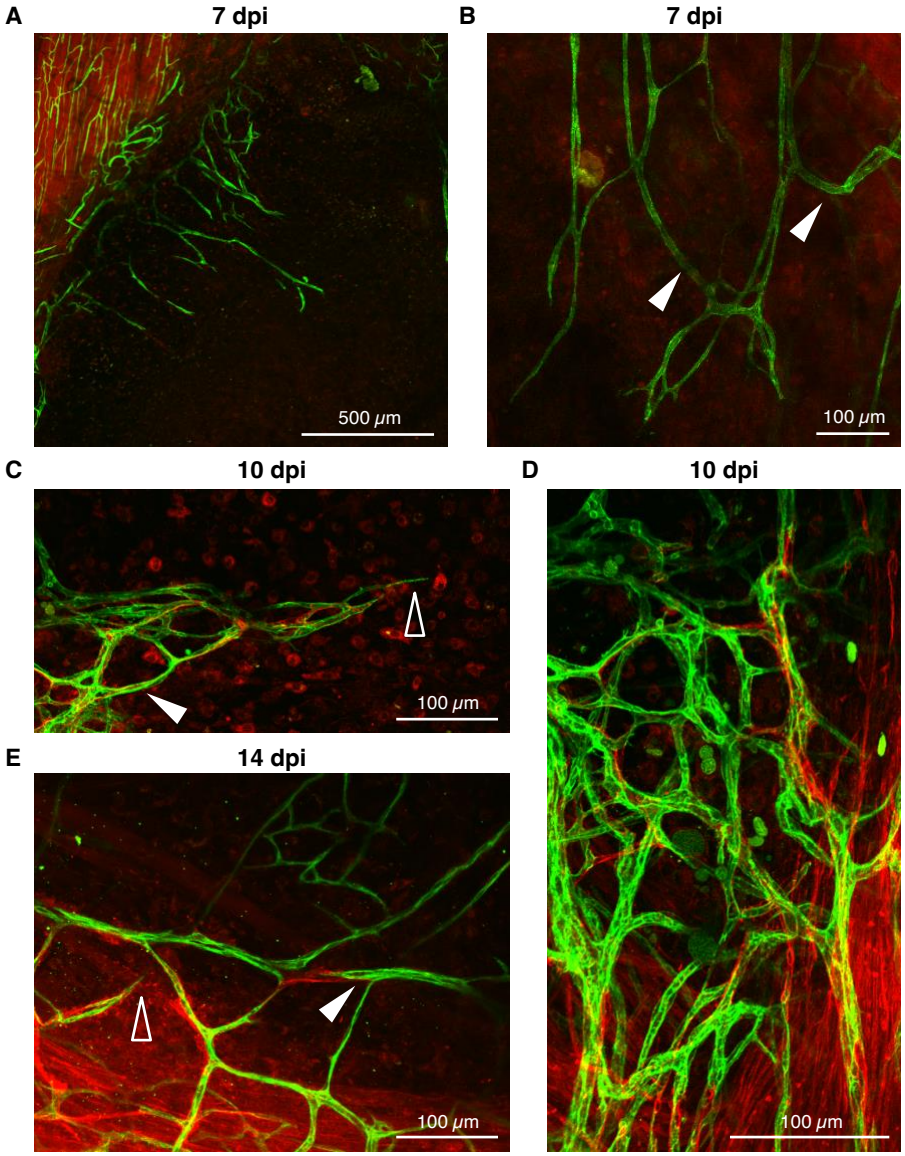

Figure 2. The microcirculation regenerates through sprouting and intussusceptive angiogenesis. **A.** At 7 dpi, nascent microvessels emigrate from existing vasculature at wound edge. **B.** At 7 dpi, microvessels are nonuniformly enlarged (arrowheads) and extend into the wound with random orientation. **C.** Intussusceptive angiogenesis (arrowhead) at 10 dpi is integral to revascularization. **D.** Zones of robust angiogenic activity at 10 dpi create irregular microvascular plexi. **E.** At 14 dpi, sprouting (open arrowhead) and intussusceptive angiogenesis (filled arrowhead) expand

regenerating microvascular networks. Images are from Cdh5-mTmG reporter mice in which ECs are green and other cells are red.

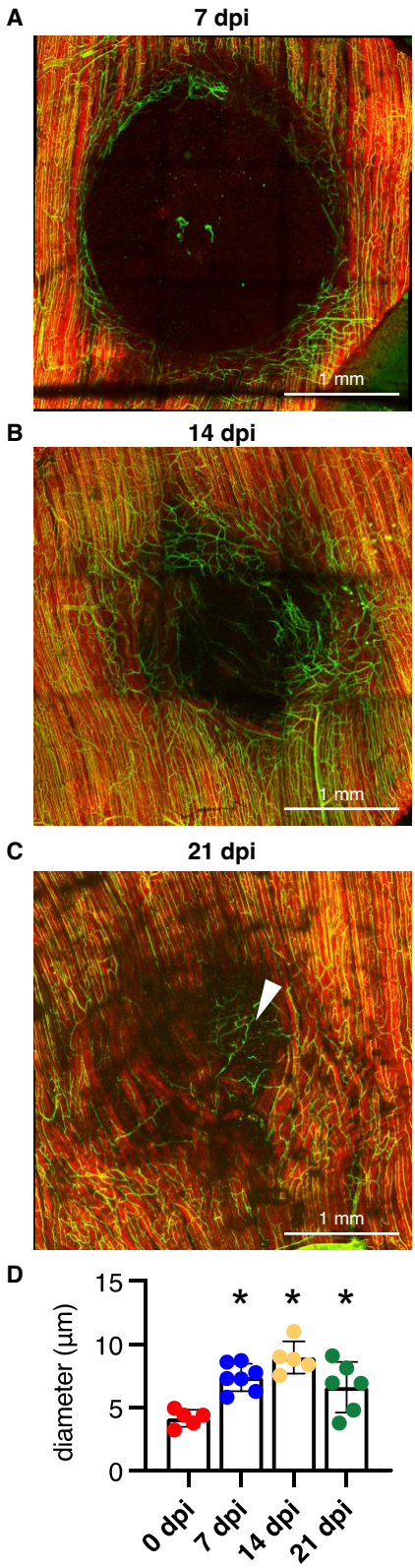

Figure 3. Time course of microvascular and myofiber regeneration after punch biopsy. **A.** At 7 dpi, angiogenesis begins at wound edges. **B.** At 14 dpi, regenerating microvessels span the wound without associated myofibers **C.** At 21 dpi, myofibers traverse the wound and microvascular networks are disorganized. Microvessels remodel to supply a cluster of adipocytes (arrowhead; not visible with reporter mice) where myofibers did not form. Images are from Cdh5-mTmG mice in which ECs are green and other cells are red. **D.** Summary data of microvessel diameters at criterion time points; n = 5-7 per time point, *P < 0.05 versus 0 dpi.

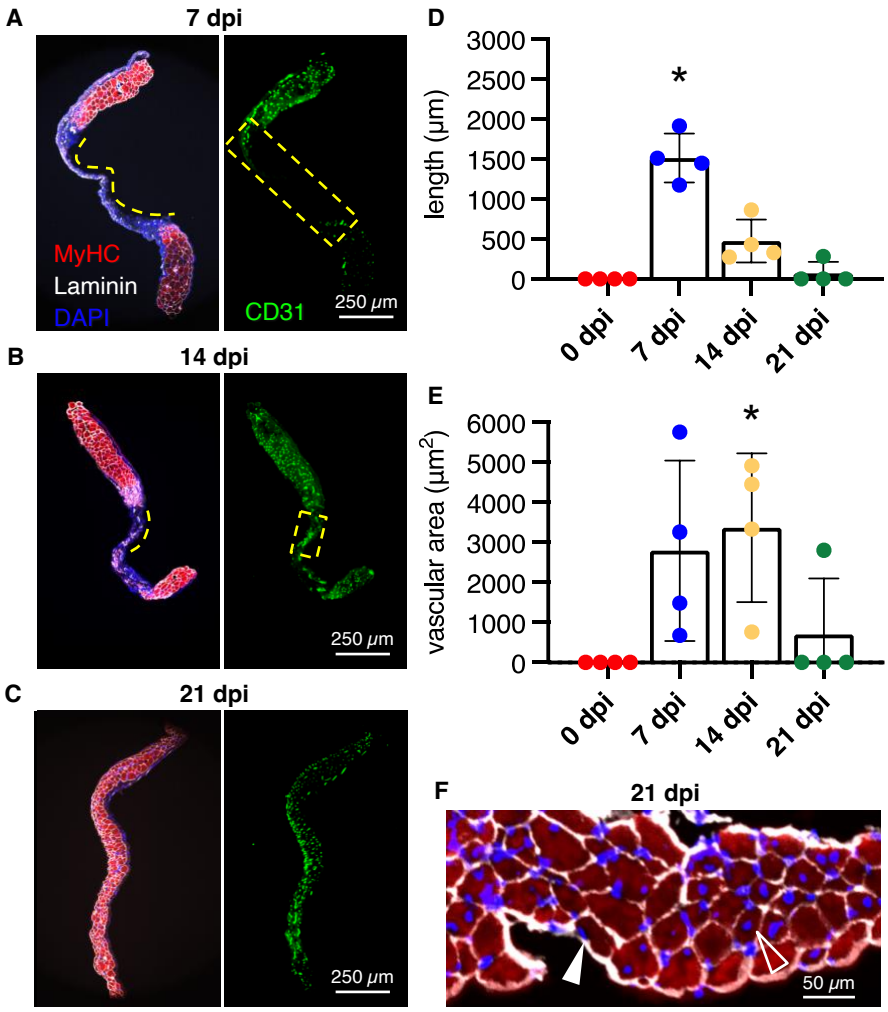

Figure 4. Angiogenesis precedes myogenesis. Representative images of GM cross sections at **A.** 7 dpi, **B.** 14 dpi, and **C.** 21 dpi. MyHC (myofibers): red; laminin (basal laminae): white; CD31 (ECs): green; nuclei: blue. **D.** Summary data for length of region devoid of myofibers (shown by broken yellow line in A and B) and **E.** Vascular area within the wound region devoid of myofibers (outlined by broken yellow box in A and B). n = 4 per time point, *P < 0.05 vs 0 dpi. **F.** Regenerated myofibers within the wound contain either central (open arrowhead) or peripherally located nuclei (filled arrowhead).

Acknowledgments

The authors thank Drs. Erika Boerman and Scott Zawieja for use of their confocal microscopes and imaging processing software. Drs. DDW Cornelison and Charles Norton for thoughtful discussion throughout data collection and analysis. Yuki Yang contributed to preliminary experiments that resulted in the punch biopsy model of injury.

Funding:

National Institutes of Health grant F32 HL-152558 (NLJ)

American Physiological Society Postdoctoral Fellowship (ABM)

National Institutes of Health Loan Repayment award (ABM)

Margaret Proctor Mulligan Fellowship, University of Missouri School of Medicine (NLJ)

Margaret Proctor Mulligan Professorship, University of Missouri School of Medicine (SSS)

School of Medicine Development Award, University of Missouri School of Medicine (SSS)

National Institutes of Health MERIT Award R37 HL-041026 (SSS)

Author contributions:

Conceptualization: NLJ, ABM, SSS

Methodology: NLJ, ABM, SSS

Investigation: NLJ, ABM, SSS

Visualization: NLJ, ABM

Funding acquisition: NLJ, ABM, SSS

Project administration: SSS

Supervision: SSS

Writing – original draft: NLJ

Writing – review & editing: NLJ, ABM, SSS

Competing interests: Authors declare that they have no competing interests.

Data and materials availability: All data are available in the main text or the supplementary materials.